Surfactant-Free Method for the Synthesis of Poly(vinyl acetate) Masterbatch Nanocomposites as a Route to Ethylene Vinyl Acetate/ Silicate Nanocomposites

Yaru Shi,† Scott Peterson, and Dotsevi Y. Sogah*

Department of Chemistry and Chemical Biology, Baker Laboratory, Cornell University, Ithaca, New York 14853-1301

Received March 11, 2006. Revised Manuscript Received January 3, 2007

Poly(vinyl acetate) (PVAc)/silicate nanocomposites have been prepared using a novel surfactant-free method comprising a copolymer of 2-(acryloxyethyl)trimethylammonium chloride (AETMC) and vinyl acetate (VAc) as the modifier for layered silicates. The nanocomposites maintained the exfoliated morphology even at silicate contents greater than 20 wt % as evidenced by the absence of peaks in the X-ray diffraction (XRD) patterns and absence of silicate bundles in the transmission electron microscopy (TEM) images. These high silicate-containing PVAc nanocomposites served as masterbatches for the preparation of ethylene vinyl acetate (EVA)/silicate nanocomposites by solution blending with EVA. A combination of XRD and TEM studies confirmed mostly exfoliated morphology for the final nanocomposites containing varying amounts of silicate. Thermogravimetric analysis (TGA) in both nitrogen and air revealed that thermal stability of the nanocomposites in air was enhanced. Dynamic mechanical analysis (DMA) of the EVA/silicate nanocomposites over a temperature range of −70 to 50 °C showed that the storage moduli of the nanocomposites above the glass transition temperature were higher than those of the pure EVA and the corresponding intercalated EVA/silicate nanocomposites. The improvement in storage modulus of the nanocomposites was attributed to the exfoliated morphology and synergistic effect of both the PVAc copolymer and the silicate. Thus, the EVA nanocomposite containing 5 wt % silicate showed a storage modulus fourfold higher than that of pure EVA and twofold higher than that of EVA/PVAc blend.

Introduction

Enhancement of properties of polymeric materials through reinforcement with inorganic fillers, such as fibers and particles of micrometer or greater dimensions, is common in the preparation of modern plastics. Advances in methods for control and modification of the nature and strength of the interactions between the polymeric and inorganic phases over large interface areas have resulted in increased attention being directed to polymer/silicate nanocomposites.[1,2] In conventional composites, enhancement in the desired materials properties is often accompanied by trade-offs in other properties.[2] For example, high content of inorganic fillers strengthen polymers but also make the materials less ductile and less tough. In contrast, nanocomposites often exhibit properties dramatically different from the micrometer scale counterparts at low inorganic contents and, sometimes but not always, without significant trade-offs. These include increased mechanical properties, decreased flammability, and increased heat distortion temperatures.[3,4] Previous studies suggest that these unique advantages of polymer/silicate nanocomposites could be attributed to the nanoscale dispersion of silicate platelets in the polymer matrix. Complete exfoliation is generally believed to best improve the properties. However, this is not always readily and reproducibly achieved using existing preparatory methods for nanocomposites.

Ethylene vinyl acetate (EVA) copolymers represent one of the most important engineering polymers and have wide applications ranging from food packaging and wire and cable insulation to melt adhesives. For most of these applications, additives often have to be used to improve both mechanical properties and fire retardancy of the EVA materials.[5] This makes EVA a good candidate for property improvement through its silicate nanocomposites.

Most of previously reported EVA nanocomposites were made by melt compounding of EVA and different alkylammonium-modified silicates.[6−16] This approach generally

* To whom correspondence should be addressed. E-mail: dys2@cornell.edu.

† Current address: CIBA Vision Corporation, Duluth, GA 30097.

(1) Ray, S. S.; Okamoto, M. *Prog. Polym. Sci.* **2003**, *28*, 1539−1641.
(2) Schmidt, D.; Shah, D.; Giannelis, E. P. *Curr. Opin. Solid State Mater. Sci.* **2002**, *6*, 205−212.
(3) Kojima, Y.; Usuki, A.; Kawasumi, M.; Okada, A.; Kurauchi, T.; Kamigaito, O. *J. Polym. Sci., Part A: Polym. Chem.* **1993**, *31*, 1755−1758.
(4) Kojima, Y.; Usuki, A.; Kawasumi, M.; Okada, A.; Fukushima, Y.; Kurauchi, T.; Kamigaito, O. *J. Mater. Res.* **1993**, *8*, 1185−1189.
(5) Beyer, G. *Fire Mater.* **2001**, *25* (5), 193−197.
(6) Zanetti, M.; Camino, G.; Mulhaupt, R. *Polym. Degrad. Stab.* **2001**, *74*, 413−417.
(7) Zanetti, M.; Camino, G.; Thomann, R.; Mulhaupt, R. *Polymer* **2001**, *42*, 4501−4507.
(8) Zanetti, M.; Kashiwagi, T.; Falqui, L.; Camino, G. *Chem. Mater.* **2002**, *14*, 881−887.
(9) Alexandre, M.; Beyer, G.; Henrist, C.; Cloots, R.; Rulmont, A.; Jerome, R.; Dubois, P. *Chem. Mater.* **2001**, *13*, 3830−3832.
(10) La Mantia, F. P.; Lo Verso, S.; Dintcheva, N. T. *Macromol. Mater. Eng.* **2002**, *287*, 909−914.

10.1021/cm060593y CCC: $37.00
Published on Web 03/07/2007

afforded intercalated or partially exfoliated morphology. A major drawback of using alkylammonium-modified silicates is their lack of adequate thermal stability that results in the decomposition and volatilization of the alkylammonium surfactants at the melt compounding and processing temperatures typically used and compromises the overall thermal stability of the nanocomposite. Furthermore, the loss of the surfactant sometimes leads to reaggregation of the silicate layers. Zanetti et al.[7] and Jeon et al.[12] have all reported reappearance of a 1.2−1.4 nm X-ray diffraction (XRD) peak after melt processing EVA/silicate nanocomposites that contained alkylammonium surfactant-modified silicates. Pramanik et al.[17−19] used solution blending of EVA with organically modified silicate and obtained nanocomposites with partial exfoliation. In addition to the volatilization problem, decomposition of the surfactant via Hoffmann elimination during melt compounding results in generation of protons on the clay surfaces, which serve as catalysts for elimination of acetic acid from EVA. This usually results in an undesirable accelerated deacetylation of EVA leading to lower decomposition temperatures.[5,7,11,13] To circumvent the volatilization problem of the small molecule surfactant modifiers, Jeon et al.[12] used maleic anhydride grafted polyethylene as a compatibilizer but obtained only partially exfoliated structure.

We have developed a surfactant-free process for preparing exfoliated masterbatch nanocomposites with high silicate content from EVA-compatible copolymers that contained pendent anchoring sites. The backbone of the polymeric modifier used in preparing the masterbatches was essentially poly(vinyl acetate) (PVAc), which is one of the few polymers miscible with EVA.[20−22] The masterbatches were then simply blended with EVA to give the final EVA/silicate nanocomposites containing the desired amounts of silicate that retained the exfoliated morphology. The method worked so well that even masterbatches that had exfoliated morphology but contained small amounts of silicate aggregates gave final nanocomposites with completely exfoliated morphology. The method enabled us to systematically vary both the polymeric modifier and silicate contents in order to fine-tune the final properties of the nanocomposites. This approach offers the opportunity to combine advantages of polymer blends and nanocomposites. We describe herein the results of our studies dealing with the synthesis of the masterbatch nanocomposites containing delaminated silicate layers modified by preformed PVAc cationic copolymers. The use of the masterbatches for the preparation of a variety of exfoliated EVA/silicate nanocomposites, thermal and dynamic mechanical properties of the nanocomposites, and the results of XRD and transmission electron microscopy (TEM) studies are also reported.

(11) Zhang, W. A.; Chen, D.; Zhao, Q.; Fang, Y. E. *Polymer* **2003**, *44*, 7953−7961.
(12) Jeon, C. H.; Ryu, S. H.; Chang, Y.-W. *Polym. Int.* **2003**, *52*, 153−157.
(13) Riva, A.; Zanetti, M.; Braglia, M.; Camino, G.; Falqui, L. *Polym. Degrad. Stab.* **2002**, *77*, 299−304.
(14) Li, X.; Ha, C.-S. *J. Appl. Polym. Sci.* **2003**, *87*, 1901−1909.
(15) Tang, Y.; Hu, Y.; Wang, S.; Gui, Z.; Chen, Z.; Fan, W. *Polym. Degrad. Stab.* **2002**, *78*, 555−559.
(16) Duquesne, S.; Jama, C.; Le Bras, M.; Delobel, R.; Recourt, P.; Gloaguen, J. M. *Compos. Sci. Technol.* **2003**, *63*, 1141−1148.
(17) Pramanik, M.; Srivastava, S. K.; Samantaray, B. K.; Bhowmick, A. K. *J. Polym. Sci., Part B: Polym. Phys.* **2002**, *40*, 2065−2072.
(18) Pramanik, M.; Srivastava, S. K.; Samantaray, B. K.; Bhowmick, A. K. *J. Appl. Polym. Sci.* **2003**, *87*, 2216−2220.
(19) Pramanik, M.; Srivastava, S. K.; Samantaray, B. K.; Bhowmick, A. K. *Macromol. Res.* **2003**, *11*, 260−266.
(20) De Souza, C. M. G.; Pacheco, C. R.; Tavares, M. I. B. *J. Appl. Polym. Sci.* **1999**, *73*, 221−226.
(21) De Souza, C. M. G.; Tavares, M. I. B. *J. Appl. Polym. Sci.* **1999**, *74*, 2990−2996.
(22) De Souza, C. M. G.; Tavares, M. I. B. *J. Appl. Polym. Sci.* **2002**, *86*, 116−124.

Experimental Section

Materials. Sodium montmorillonite (MMT) with a cationic exchange capacity of 90 mequiv/100 g was purchased from Southern Clay Products. XRD gave the *d* spacing of the interlayer as 1.2 nm. Vinyl acetate (VAc) was purchased from Aldrich and purified by distillation under reduced pressure. The EVA copolymer used contained 39 wt % VAc (Exxon Mobil's Escorene, UL05540EH2, VAc39%). 2-(Acryloxyethyl)trimethylammonium chloride (AETMC) was purchased from Aldrich and recrystallized once from acetone. Azobis(isobutyronitrile) (AIBN) was recrystallized twice from methanol. All other reagents and solvents were ACS grade purchased from Aldrich and used without further purification. Detailed experimental procedures are provided as Supporting Information. Only typical procedures are given in the manuscript.

Characterization. XRD was performed on powder samples on a Scintag X-ray diffractometer in $\theta-\theta$ geometry using Cu Kα radiation ($\lambda = 1.54$ nm) operated at 45 kV and 40 mA. The scanning speed and the step size used were 3°/min and 0.02°, respectively. Scanning transmission electron microscopy (STEM) was performed on a 100 keV HB501/UX dedicated ultrahigh vacuum scanning transmission electronic microscope (UHV-STEM). Both bright field and annular dark field images were taken using a digital camera. The specimens were prepared by grinding the sample in liquid nitrogen in an Agate mortar, and the fine powder was then soaked in either isopropanol or methanol and picked up onto a 300 Å mesh holey carbon film copper grid. TEM was performed on LEO 922 EFTEM. The specimens were embedded in Tissue-Tek O.C.T. compound glue followed by microtoming at −55 °C using a Leika Ultracut UCT (M.O.C., Inc.). The specimens were 85 nm thick and were picked up from dimethylsulfoxide onto copper grids. ^{1}H NMR was carried out on 400 MHz INOVA spectrometer. Molecular weights were determined with respect to polystyrene standards using size exclusion chromatography (SEC) in tetrahydrofuran (THF) on Waters HPLC with Ultrastyragel (Waters Associates) columns and both refractive index and UV detectors. Unless otherwise specified, thermogravimetric analysis (TGA) was performed on a Seiko thermogravimetric differential thermal analyzer under both N_2 and air flow within a temperature range of 25−550 °C at a heating rate of 10 °C/min. The residual silicate (wt %) was calculated from the TGA data at 525 °C. At this temperature, the weight loss of the polymer in the nanocomposite was complete, but the MMT showed negligible weight loss (in a separate run). The residual wt % of the polymer (separately measured by TGA under the same conditions) was subtracted from the residual wt % of the nanocomposite to obtain the silicate content of the nanocomposite. Dynamic mechanical analysis (DMA) was carried out on TA Instruments dynamic mechanical analyzer DMA 2980 at a fixed frequency of 1 Hz, within a temperature range of −70 to 50 °C and at a heating rate of 3 °C/min. The specimens for DMA were prepared by compression molding of ground samples at 67 °C into a 30 mm × 5 mm × 1 mm stainless steel mold at a pressure of 5 psi followed by cooling at room temperature.

Copolymerization of VAc with AETMC. A 500-mL three-neck round-bottom flask, equipped with a mechanical stirrer, a nitrogen

Scheme 1. Synthesis of the Cationic PVAC Copolymers

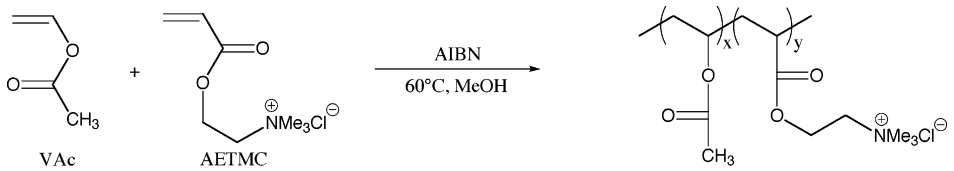

PVAc-A: x = 99.63, y = 0.37 mol%, M_w = 130,000, M_n = 63,000
PVAc-B: x = 99.00, y = 1.00 mol%; M_w = 102,000, M_n = 57,000
PVAc-C: x = 97.90, y = 2.14 mol%; M_w = 66,000, M_n = 21,000

gas inlet, and an addition funnel containing AETMC (1.00 g, 5.16 mmol) dissolved in methanol (14 mL), was charged with distilled VAc (100.00 g, 1.16 mol), AETMC (0.06 g, 0.31 mmol), and degassed methanol (33 mL). Nitrogen was bubbled through the mixture in the flask for 30 min while stirring at a speed of 100 rpm. The mixture was heated to 60 °C with constant stirring. AIBN (0.96 g, 5.82 mmol) was then added. Addition of the methanol solution of AETMC in the addition funnel was begun and continued throughout the course of the polymerization, which lasted for 1.5 h. The reaction mixture, which had turned viscous and a little cloudy, was cooled to room temperature, diluted with acetone (250 mL), and poured into hexanes (2 L). The tacky precipitate that formed was isolated by decanting off the solvents. The isolated polymer was dissolved in methanol (500 mL) and poured into a large amount of cold water (approximately 8−10-fold) to precipitate the polymer as a white solid. (Note: Sometimes it was found convenient to perform the precipitation in 1-L batches.) The precipitation from the methanol/water mixture was repeated once, and the isolated solid polymer was dried in a vacuum oven at 50 °C overnight to give the copolymer designated PVAc-A. Yield: 32 g (32%). Composition of the copolymer by ^{1}H NMR: calcd for AETMC, 0.45 mol %; found, 0.37 mol %. GPC: M_n = 63 000, M_w = 130 000.

PVAc-C. A 500-mL three-neck round-bottom flask, equipped with a mechanical stirrer, a nitrogen gas inlet, and a syringe pump containing AETMC (16.00 g, 82.61 mmol) dissolved in degassed methanol (28 mL), was charged with distilled VAc (100.00 g, 1.16 mol), AETMC (0.96 g, 4.96 mmol), and degassed methanol (66 mL). Nitrogen was bubbled through the mixture in the flask for 30 min while stirring at a speed of 100 rpm. The mixture was heated to 60 °C with continued stirring. AIBN (0.96 g, 5.82 mmol) was added. The addition of the methanol solution of AETMC in the syringe pump was begun at 0.2 mL/min and continued over a 3-h period. The reaction was stirred at 60 °C for an additional 1 h. The reaction mixture, which has turned viscous and a little cloudy, was cooled to room temperature, diluted with acetone (250 mL), and poured into hexanes (2 L). The solvents were decanted off to give a tacky precipitate, which was dissolved in methanol (500 mL) and poured into cold water (1 L). A white sticky suspension resulted that could not be readily filtered. This was therefore centrifuged (in 200-mL batches) at 7000 rpm for 30 min, and the solvents were decanted off. The resulting solid was triturated with water (400 mL), centrifuged, and filtered. The trituration with water and centrifuging was repeated once, and the isolated solid was dried in a vacuum oven at 50 °C overnight. Yield: 59 g (51%). Composition by ^{1}H NMR: calcd for AETMC, 7.2 mol %; found, 2.14 mol %. GPC: M_n = 21 000, M_w = 66 000.

Homopolymerization of VAc. A 500-mL three-neck round-bottom flask, equipped with a mechanical stirrer and a nitrogen gas inlet, was charged with distilled VAc (100.00 g, 1.16 mol) and degassed methanol (33 mL). Nitrogen was bubbled through the mixture in the flask for 30 min while stirring at a speed of 100 rpm. The mixture was heated to 60 °C followed by addition of AIBN (0.96 g, 5.82 mmol). The stirring was continued at 60 °C for a total reaction time of 1.5 h. The reaction mixture was cooled to room temperature, diluted with acetone (250 mL), and poured into hexanes (2 L). The precipitate that formed was isolated by decanting off the solvents, dissolving the residue in methanol (500 mL), and pouring the resulting solution into a large amount of cold water (approximately 8−10-fold) to precipitate the polymer as a white solid. The precipitation from the methanol/water mixture was repeated once. The white solid was dried in a vacuum oven at 50 °C overnight to give PVAc. Yield: 50 g (50%). GPC: M_n = 54 000, M_w = 129 000.

PVAc/MMT Masterbatch Nanocomposite. A typical procedure is as follows: A 1-L Erlenmeyer flask was charged with PVAc-A (12 g) and methanol (600 mL). To this solution, MMT (3 g) dispersed in 150 mL of water was added slowly with stirring. The mixture was heated to 50 °C, stirred for 4 h, cooled to room temperature, and transferred into a round-bottom flask. The methanol was removed as completely as possible using a rotatory evaporator to give an aqueous suspension. This was filtered, and the resulting white precipitate was washed with water and dried overnight in a vacuum oven at 50 °C to give a white solid, designated PVAc-A20. Yield: 12.0 g (80%). TGA: calcd for silicate, 20 wt %; found, 20.5 wt %. First onset decomposition temperature (T_{d1}), 306 °C. Second onset decomposition temperature (T_{d2}), 424 °C. XRD: *d* spacing, 2.0 nm. For PVAc-A05 and others, see Supporting Information.

EVA/Silicate Nanocomposites. To a 500-mL Erlenmeyer flask, containing a magnetic stirring bar, were added PVAc-B20 masterbatch (5 g) and THF (250 mL). The dispersion was stirred overnight at room temperature and then sonicated for 1 h. A separate 500-mL round-bottom flask was charged with EVA (15 g) and THF (100 mL). To this solution was added the preformed masterbatch dispersion. The reaction mixture was heated to 50 °C and maintained at this temperature with stirring for 4 h. After it was allowed to cool to room temperature, the mixture was evaporated in vacuo to dryness. The resulting nanocomposite, designated EVA-NC5, was dried overnight in a vacuum oven at 50 °C. Yield: Quantitative. TGA: calcd for silicate, 5.5 wt %; found, 5.6 wt %. T_{d1} = 311 °C. T_{d2} = 445 °C. XRD: no peak. For EVA-NC1 and others, see Supporting Information.

Results and Discussion

Copolymerization of VAc with AETMC. The copolymers were prepared by traditional free radical copolymerization techniques (Scheme 1). The order of addition of the monomers was dictated by the relative reactivities of AETMC (M1, r_1 = 22.2) and VAc (M2, r_2 = 0.03) in methanol.[23] As a result of the large disparity between the reactivities of the monomers, the more reactive monomer

Table 1. Results of the Copolymerization of VAC and AETMC

	comonomer							TGA[h] (under N_2)	
sample	PVAc (M2), g (mol)	AETMC (M1), g (mmol)	yield (%)	f_1 AETMC[a] (mol %, feed)	F_1 AETMC[b] (mol %, obsd)	M_w[c] ($\times 10^{-3}$)	M_n[c] ($\times 10^{-3}$)	T_{d1}[e]	T_{d2}[f]
PVAc	100.00 (1.16)	N/A[d]	50	0	0	129	54	315	419
PVAc-A	100.00 (1.16)	1.06 (5.47)	32	0.45	0.37	130	63	316	426
PVAc-B	100.00 (1.16)	8.48 (43.79)	28	3.60	1.00	102	57	314	426
PVAc-C	100.00 (1.16)	16.96 (87.57)	50	7.20	2.14	66	21	ND[g]	ND[g]

[a] Relative amount of cationic monomer in the feed in mol %. $f_1 + f_2 = 1$. [b] Observed relative amount of cationic monomer in the copolymer in mol % measured by ^{1}H NMR. $F_1 + F_2 = 1$. [c] Molecular weights determined by SEC with respect to polystyrene standard. [d] Not applicable. [e] First onset decomposition temperature. [f] Second onset decomposition temperature. [g] Not determined. [h] All data were on Seiko Instruments equipment except PVAc-B, which was analyzed on TA Instruments equipment.

(M1) was continuously fed to the reactor containing the less reactive VAc (M2) via either an addition funnel or syringe pump.[23,24] This was a modification of the so-called "comonomer-feeding method" used by Moritani and Yamaguchi[23] to prepare PVAc modified with cationic acrylamide comonomers.

The copolymer was first precipitated from acetone/hexanes in order to remove unreacted VAc and then from cold methanol/water twice to remove traces of unreacted cationic monomer and any AETMC homopolymer. The yields (Table 1) varied from 28−50%, consistent with the yield of 41% reported in the literature.[23]

Table 1 summarizes the copolymerization results. Copolymer compositions were determined by ^{1}H NMR. The relative molar amount of AETMC incorporated into the copolymer (F_1) was calculated from the integral of the trimethylammonium protons at 3.45 ppm relative to the methine ester hydrogen (−CH−O−) of PVAc at 4.82 ppm. In all cases, the cationic monomer content (F_1) in the copolymer was less than that in the feed (f_1). We attribute this to the aforementioned disparity in the reactivity ratios of the monomers and the fact that the reaction is not a living polymerization and, consequently, give incomplete conversion of monomers. This is typical for traditional free radical polymerization of VAc. It can be shown from the reactivity ratios that the rate constant of the cationic homopolymer formation k_{11} is 22-fold higher than the crossover rate constant k_{12} and that the second crossover rate constant k_{21} is about 33 (1/0.03) times the VAc homopolymerization rate constant k_{22}.[25] These values suggest that some AETMC homopolymer could form during the polymerization. However, any homo-AETMC produced would have been removed by the water wash during workup because of its high solubility in water. This would lead not only to lower copolymer yields but also to lower mol % of AETMC incorporated into the copolymer as indicated by the F_1 values in Table 1. The higher the AETMC content in the copolymer, the more water-soluble it became and the more difficult it was to isolate the copolymer. For example, PVAc and PVAc-A (Table 1, entry 2) precipitated very easily from water while PVAc-B (Table 1, entry 3) formed a soft, sticky white solid but could still be isolated by precipitation from large amounts of cold water. In contrast, PVAc-C (Table 1, entry 4) formed a homogeneous suspension in water and could only be isolated after centrifuging.

Scheme 2. Synthesis of the PVAC/Silicate Masterbatch Nanocomposites

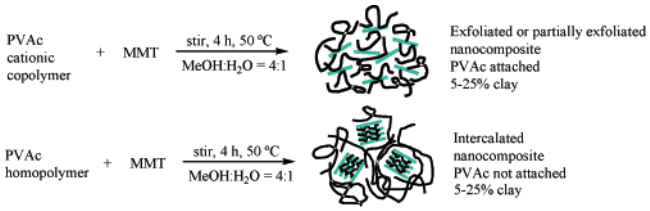

Synthesis, Characterization, and Morphology of PVAc/Silicate Masterbatch Nanocomposites. The masterbatches were prepared by adding a dispersion of MMT in water to a solution of the copolymer in methanol and heating the mixture at 50 °C for 4 h. After removal of the methanol using a rotatory evaporator and washing the resulting precipitate thoroughly with water, the nanocomposites were isolated as white powder. The synthesis of the masterbatch is outlined in Scheme 2, and the results are summarized in Table 2.

The yields varied from 64 to 94%. The less than quantitative yields were due to several factors. (1) Many of the reactions were performed on a very small scale (50−100 mg of MMT). (2) The isolation in some cases required using large amounts of solvents. (3) The copolymers were soluble to varying extents in water. Hence, we were not able to determine with any accuracy if the rest of the material was polymer, clay, or both. However, the fact that in every case the wt % MMT obtained by TGA is higher than the calculated value (Table 2) rules out loss of clay only being the culprit. Loss of both components, that is, loss of the nanocomposite, should also not cause a significant change in the experimental MMT contents (TGA values) relative to the calculated values. In order to determine how loss of polymer would affect the results, we compared the observed silicate content as measured by TGA with what would be expected if the loss in yield were mainly due to polymer loss. For the A-series nanocomposites, these "expected" values were 7.5, 11.9, and 24.0 wt % for EVA-A05, -A10 and -A20, respectively, which clearly differ from both the calculated values based on the actual amounts of materials used (5, 10, and 20 wt % (Table 2)) and the observed (TGA) values of 5, 9.1, and 20.5 wt %, respectively. Similarly, for EVA-B05, EVA-B10, and EVA-B20, the observed values of 5.9, 11.8 and 21.9 wt % are closer to the calculated values in Table 2 than the values of 7.6, 14.7, and 22.3 wt %,

(23) Moritani, T.; Yamaguchi, J. *Polymer* **1998**, *39* (3), 559−572.
(24) Hanna, R. J. *Ind. Eng. Chem.* **1957**, *49*, 208−209.
(25) Chalais, S.; Laszlo, P.; Mathy, A. *Tetrahedron Lett.* **1986**, *27*, 2627−2630.

Table 2. Characteristics of Polymer/Silicate Masterbatch Nanocomposites[a]

masterbatch[a]	polymer (g)	AETMC wt,[b] mg (mmol)	MMT wt,[c] g (mequiv)	% yield	MMT wt % (calcd)	TGA[h] (under N_2) MMT wt %	T_{d1}[d] (°C)	T_{d2}[e] (°C)	XRD *d* spacing[f] (nm)
PVAc-A05	PVAc-A (0.95)	7.90 (0.041)	0.05 (0.045)	65	5	5.3	309	417	no peak
PVAc-A10	PVAc-A (0.90)	7.47 (0.039)	0.10 (0.090)	82	10	9.1	309	418	br sh[f]
PVAc-A20	PVAc-A (12.0)	99.60 (0.51)	3.00 (2.70)	79	20	20.5	306	424	2.0
PVAc-B05	PVAc-B (0.95)	21.19 (0.11)	0.05 (0.045)	64	5	5.9	313	416	no peak
PVAc-B10	PVAc-B (0.90)	20.07 (0.10)	0.10 (0.90)	64	10	11.8	306	418	no peak
PVAc-B20	PVAc-B (12.0)	267.60 (1.38)	3.00 (2.70)	87	20	21.9	303	423	2.4 (br sh)[f]
PVAc-C20	PVAc-C (40.0)	1880 (9.71)	10.00 (9.00)	94	20	24.9	308	417	no peak
PVAc-05	PVAc (0.95)	N/A[g]	0.05 (0.045)	75	5	5.8	315	418	v small; br[f]
PVAc-10	PVAc (0.90)	N/A[g]	0.10 (0.090)	76	10	13.7	309	420	2.1
PVAc-20	PVAc (12.0)	N/A[g]	3.00 (2.70)	82	20	24.4	305	428	2.1

[a] From the molecular weight and F_1 values, we calculated the wt % of AETMC to be as follows: PVAc-A, 0.83 wt %; PVAc-B, 2.23 wt %; PVAc-C, 4.70 wt %. PVAc made up the remaining wt %. [b] Millimoles of ammonium cationic sites in the copolymer calculated from the corresponding wt % of AETMC in the copolymer and the molecular weight of AETMC. [c] Calculated from the 0.90 mequiv/g cation exchange capacity of the original clay. The numbers in parentheses represent the millimoles of cations that could be replaced by the ammonium cation of AETMC. [d] First decomposition temperature. [e] Second onset decomposition temperature. [f] br = broad, sh = shoulder. [g] Not applicable. [h] All samples were analyzed on Seiko Instruments equipment except PVAc-A05, PVAc-A10, and PVAc-A20, which were analyzed on TA Instruments equipment.

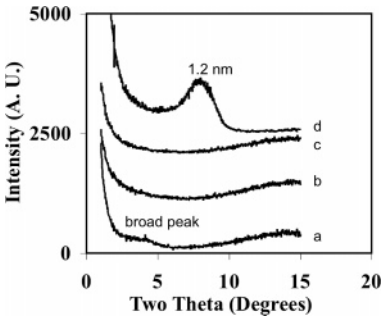

Figure 1. XRD plots of PVAc masterbatch nanocomposites. (a) PVAc-05, (b) PVAc-A05, (c) PVAc-B05, and (d) MMT.

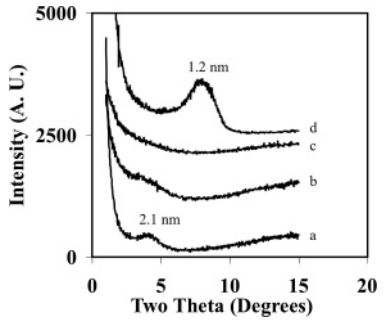

Figure 2. XRD plots of PVAc masterbatch nanocomposites. (a) PVAc-10, (b) PVAc-A10, (c) PVAc-B10, and (d) MMT.

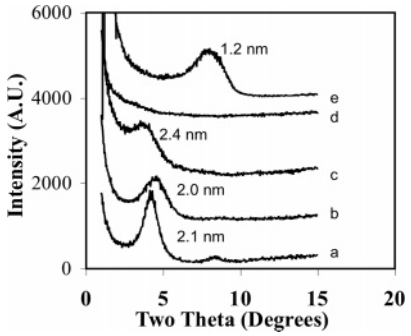

Figure 3. XRD plots of PVAc masterbatch nanocomposites. (a) PVAc-20, (b) PVAc-A20, (c) PVAc-B20, (d) PVAc-C20, and (e) MMT. Numbers on the plots correspond to the *d* spacing represented by each main peak.

respectively, calculated by assuming polymer only loss. This suggests that the yield losses in both series could not be due to loss of polymer only but rather to losses in both clay and polymer during the isolation process, possibly because of the aforementioned inherent difficulty involved in handling the nanocomposites on such small scales and the large amounts of solvents used both for the reaction and the product isolation. Applying the same analysis to the nanocomposites made from homo-PVAc, we, however, found that in two cases (PVAc-10 and PVAc-20) it appeared more polymer than clay was lost. This could be because PVAc does not interact with the clay as strongly as does the copolymer and, therefore, is more likely to come off during isolation. In the case of PVAc-C20, it appears that because of the relatively high aqueous solubility of the copolymer the loss in yield was mainly due to loss of the copolymer.

Figure 1 presents the XRD patterns of PVAc/silicate masterbatches containing about 5−6% silicate. The XRD plot for the microcomposite prepared from PVAc homopolymer (PVAc-05) clearly showed a diffraction peak at $2\theta = 4.2°$ (*d* spacing 2.1 nm) due to the *d*001 basal reflection, indicating an intercalated structure. In contrast, the XRD plots for the copolymer/silicate nanocomposites (PVAc-A05 and PVAc-B05) showed no diffraction peaks, indicating possible exfoliation of the silicate.

When the silicate content was increased to 9−14% (Figure 2), the nanocomposite containing the lowest amount of the cationic copolymer (0.37 mol %; PVAc-A10) gave a very broad small shoulder between 3 and 5° that was not well-defined, suggesting that the silicate layers are mostly exfoliated. The one containing the higher cationic moiety (1.00 mol %; PVAc-B10) gave no peak in the XRD plot, which suggests that the layers are fully exfoliated. As expected, the masterbatch from homo-PVAc (PVAc-10) showed a peak (*d* spacing of 2.1 nm) that indicates that this masterbatch is intercalated. With further increase in the silicate content to 20−24%, sharper peaks at 4.2° (*d* spacing of 2.1 nm) were observed for both PVAc-20 and PVAc-A20 (Figure 3). In the case of homopolymer masterbatch (PVAc-20), a peak occurred at 8.3° (*d* spacing 1.2 nm) and is, therefore, attributed to silicate bundles from the original MMT that did not exfoliate, possibly as a result of the high MMT content and absence of strongly interacting polymer chains. In the XRD of the nanocomposite containing higher

cationic moiety (PVAc-B20, 1.00 mol % AETMC) a broad small shoulder appeared at 4° (approximate *d* spacing of 2.4 nm), but the reappearance of the original MMT peak was not observed. The presence, location, and *d* spacing of the shoulder suggest that PVAc-B20 contained some intercalated material, albeit very small, with an expanded interlayer spacing (2.4 nm versus 2.1 nm for PVAc-A20). For the masterbatch containing the highest amount of cationic comonomer (PVAc-C20, 2.14 mol % AETMC), the XRD showed no peak, which indicates that the silicate layers are fully exfoliated. It can be concluded from the results presented so far that the extent of exfoliation depends on many factors, including the silicate loading and the extent to which the polymer interacts with the silicate layers, which, in turn, is determined by the milli-equivalents of cationic sites in the polymeric modifier.

The differences in the XRD patterns could be explained by the fact that in the nanocomposites containing no cationic comonomer (PVAc-05, -10, and -20) the PVAc homopolymer chains interacted with the silicate layers via mainly van der Waals forces; however, in the nanocomposites containing cationic units (PVAc-A, PVAc-B, and PVAc-C series) strong electrostatic interactions were at play. Because the extent of exfoliation depends on the amount of AETMC in the copolymer, we calculated the millimoles of ammonium cationic sites incorporated (Table 2, column 3, numbers in parentheses) and compared the values to the milli-equivalents of exchangeable cationic sites in the clay (Table 2, column 4, numbers in parentheses). Examination of the data in columns 3 and 4 revealed that in PVAc-A05 the millimoles of AETMC used represented 91% of the total milli-equivalents of exchangeable cations in the clay. However, in PVAc-A10 and PVAc-A20 the corresponding percentages were 43 and 19%, respectively. Hence, in the A-series, only the A05 sample showed evidence of complete exfoliation while A10, although mostly exfoliated, contained some intercalated layers as evidenced by the broad ill-defined shoulder in the XRD. Further examination of the data showed that PVAc-B05, PVAc-B10, and PVAc-C20, all of which showed no peak in the XRD plots, contained millimoles of ammonium cation sites that were in excess over the milli-equivalents of the exchangeable inorganic cations in the clay: 244, 111, and 109%, respectively. In contrast, PVAc-B20, which showed a small broad shoulder (*d* spacing 2.4 nm) in the XRD plot, contained cationic sites that were 51% of the milli-equivalents of the exchangeable cations in the clay. The overall internal consistency of the data suggests that in order for the nanocomposite to give evidence of complete exfoliation (no peaks) in the XRD, the number of AETMC cationic groups must be greater than 50% and, preferably, as close as possible to the milli-equivalents of exchangeable cations in the clay. Between approximately 40 and 50% exchange, some intercalated structure may form. On the basis of the above XRD results, it is reasonable to conclude that incorporation of cationic sites into PVAc facilitated strong interactions of the polymer chains with the silicate surface, thereby leading to the silicate platelets becoming either disordered or exfoliated or having expanded galleries with *d* spacings out of the detection range of the diffractometer. The higher the cationic content, the greater was the effect.

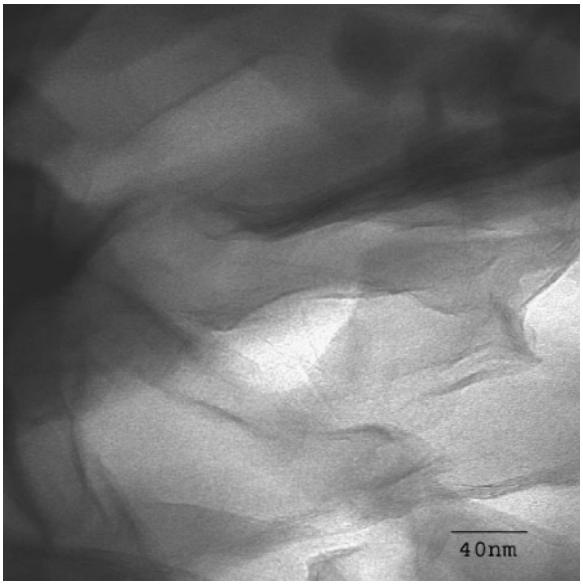

Figure 4. STEM of PVAc-10.

Although XRD is a powerful method for characterizing the structure of nanocomposites, there is evidence in the literature suggesting that the mere absence of peaks in the pattern is not sufficient to draw conclusive inferences regarding complete exfoliation and that corroborative evidence from other sources is necessary. Hence, in order to confirm the deductions from the above XRD results, we performed STEM and TEM measurements on the nanocomposites containing about 10% silicate (STEM for PVAc-10 and PVAc-A10 and TEM for PVAc-B10) as representative examples and compared the results with the XRD of Figure 2. The STEM image of PVAc-10 (Figure 4) showed large silicate stacks, which might be responsible for the peak at 4.2° in the XRD (Figure 2). The *d* spacing (2.1 nm) of the silicate layers of this sample suggests that the stacks are intercalated with PVAc. Obviously, the non-cationic PVAc homopolymer is hydrophilic enough to have some compatibility with the pristine MMT, leading to an intercalated morphology. The interactions between the silicate and the polar ester groups along the PVAc homopolymer chain permitted one or two layers of polymer chains to be incorporated into the hydrophilic silicate intergallery as diagrammed in Scheme 2.

The STEM image of the nanocomposite containing 0.37% cationic moiety (PVAc-A10) showed mostly single silicate platelets, which is consistent with exfoliation (Figure 5), despite the presence of a broad shoulder in the XRD (Figure 2). This is important especially since the material contained only 43% AETMC cations relative to the milli-equivalents of exchangeable cations in the clay. The broad shoulder (Figure 2) could be due to a small amount of stacked silicate layers, although these could not be readily discerned from the STEM image.

Figure 6 shows the low magnification TEM image of PVAc-B10, the nanocomposite with higher cationic anchoring sites (111% relative to milli-equivalents of exchangeable cations of the clay). Clearly, the original stacked silicate

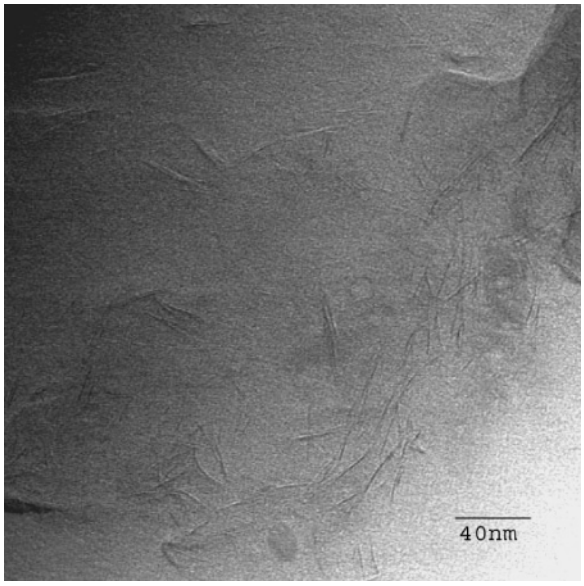

Figure 5. STEM of PVAc-A10.

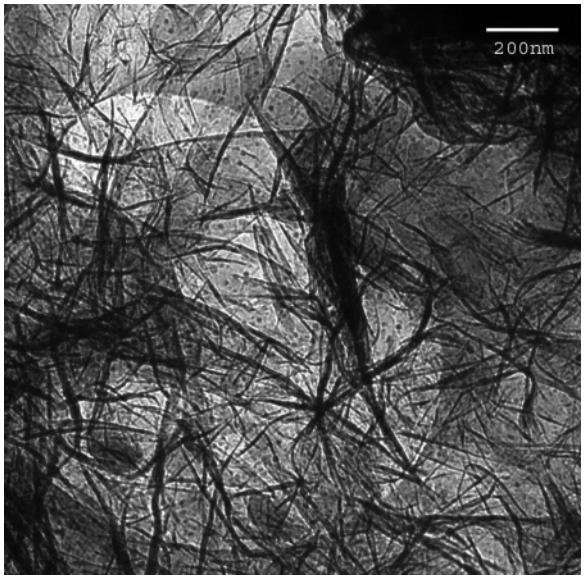

Figure 6. Low magnification TEM of PVAc-B10.

layers were exfoliated into single (or, at most, double) silicate layers that were uniformly distributed within the polymer matrix. The dark area in the center of the image was caused by the nonuniform thickness of the TEM specimen. Overall, evidence for exfoliated morphology of PVAc-B10 is overwhelming, which is consistent with the XRD patterns in Figure 2. Hence, both XRD and electron microscopy indicated that incorporation of cationic moieties into the polymer made it possible for the polymer to become attached to the silicate surface, and this facilitated exfoliation.

Thermal Properties of the PVAc/Silicate Masterbatch Nanocomposites. Figures 7 and 8 show representative TGA curves obtained under N_2 for PVAc/silicate and PVAc-B/silicate masterbatch nanocomposites, respectively. The TGA curves showed that both the intercalated (homo-PVAc series) and the exfoliated (exemplified by PVAc-B series) nanocomposite gave similar decomposition profiles and that the degradation of PVAc took place in two stages. The first (T_{d1}) and the second onset (T_{d2}) decomposition temperatures are summarized in Table 2. In general, T_{d1} for the master-

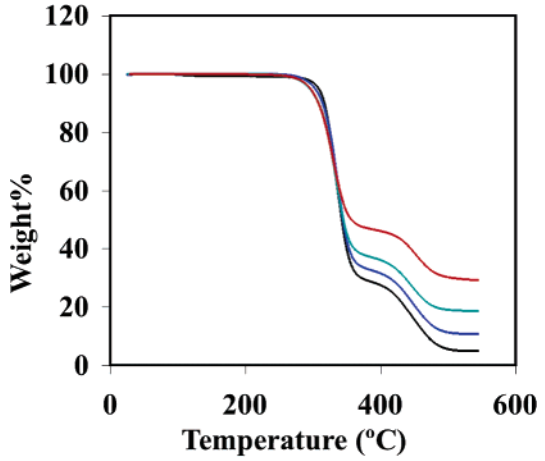

Figure 7. TGA of PVAc (black), PVAc-05 (blue), PVAc-10 (green), and PVAc-20 (red) in N_2.

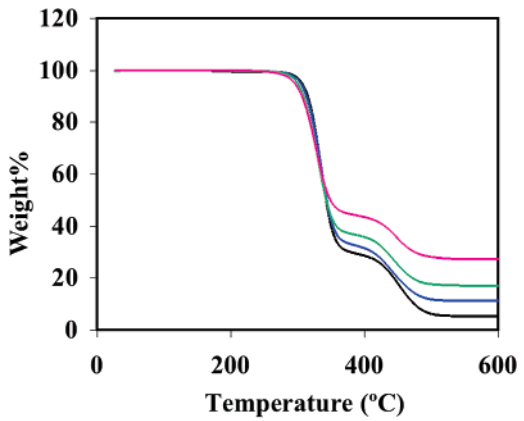

Figure 8. TGA of PVAc-B (black), PVAc-B05 (blue), PVAc-B10 (green), and PVAc-B20 (red) in N_2.

batch nanocomposites occurred at temperatures (about 303−313 °C) slightly lower (by 2−12 °C) than T_{d1} of PVAc in absence of clay (315 °C, Table 1). The lower decomposition temperature is attributed to deacetylation of VAc groups (elimination of acetic acid) to form polyacetylene segments in the backbone.

The difference between T_{d1} of the nanocomposite and that of the free polymer became more pronounced as the silicate content was increased. For example, T_{d1} for masterbatches prepared from PVAc-B and from the homo-PVA decreased by 12 and 10 °C, respectively, upon increasing the clay content to about 20 wt %. This slight but reproducible decrease in the temperature at which the elimination of acetic acid ensued might be due to the well-established Lewis and/or Brønsted acid catalysis by the layered silicate.[25−27] The change in the T_{d1} of the mostly intercalated PVAc-A series nanocomposites as a function of silicate content was much smaller (3 °C) than observed for the exfoliated PVAc-B series. A closer examination of the thermograms revealed that the slope of the deacetylation curve decreased slightly in going from pure PVAc to the nanocomposites, becoming more gradual with increasing silicate content (see Supporting Information). For the PVAc-B series the slope in wt %/°C

(26) Pitchumani, K.; Pandian, A. *J. Chem. Soc., Chem. Commun.* **1990**, *22*, 1613−1614.
(27) Hunter, D. B.; Bertsch, P. M. *Environ. Sci. Technol.* **1994**, *28*, 686−691.

Table 3. EVA/Silicate Nanocomposites Prepared from the Masterbatches[a]

nanocomposite designation	masterbatch or polymer, wt (g)	EVA wt (g)	PVAc or copolymer (wt %)	MMT (wt %; calcd)	TGA		
					MMT (wt %)	T_{d1}[d] (°C)	T_{d2}[e] (°C)
EVA	N/A[c]	N/A[c]	0	0	0	322	442
EVA-1	PVAc-20 [20.5][b] (1)	19	4	1.0	0.9	318	443
EVA-2	PVAc-20 (2)	18	8	2.1	1.9	321	443
EVA-5	PVAc-20 (5)	15	20	5.1	5.9	311	444
EVA-0	PVAc (4)	16	20	0	0	309	433
EVA-NC1	PVAc-B20 [21.9][b] (1)	19	4	1.0	0.84	319	444
EVA-NC2	PVAc-B20 (2)	18	8	2.2	2.1	318	444
EVA-NC5	PVAc-B20 (5)	15	20	5.5	5.6	311	445
EVA-NC0	PVAc-B (4)	16	20	0	0	309	435

[a] The first decomposition temperatures of the masterbatches are provided in Table 2. [b] Numbers in brackets denote actual silicate percentages in the masterbatches. [c] Not applicable. [d] First onset decomposition temperatures under nitrogen. [e] Second onset decomposition temperatures under nitrogen.

decreased from 1.77 for PVAc-B (no clay) to 1.68 (PVAc-B05), 1.38 (PVAc-B10), and 1.24 (PVAc-B20). For homo-PVAc series the corresponding values are 1.83 (PVAc), 1.72 (PVAc-05), 1.38 (PVAc-10), and 1.20 (PVAc-20). This suggests that the escape of the eliminated volatiles from the nanocomposites is somewhat impeded by the silicate layers and that this effect appears to be independent of the extent of exfoliation as both the exfoliated PVAc-B masterbatches and the intercalated PVAc microcomposites exhibit the same trend. This might have a beneficial effect on the flame retardant properties of the nanocomposites. The improved thermal stability is further demonstrated by the fact that the curves showed increase in the residue at high temperatures.

The second onset decomposition temperatures (T_{d2}), corresponding to degradation of the polymer backbone, increased from 418 to 428 °C for the microcomposites (Figure 7), 416 to 423 °C for the exfoliated PVAc-B masterbatches (Figure 8), and 417 to 424 °C for the intercalated PVAc-A masterbatches (see Supporting Information). This suggests that the thermal stability of the main chain, unlike the deacetylation process, is either slightly enhanced or, at least, not adversely affected by the presence and the amount of the silicate. The higher the silicate content, the slower the rate of escape of degradation products as evidenced by the gradual decrease in slope of the degradation curve as the silicate content was increased. For example, for the PVAc-B series the slope (wt %/°C) decreased from 0.39 for PVAc-B containing no silicate to 0.31 (PVAc-05), 0.30 (PVAc-10), and 0.27 (PVAc-20). A similar trend was observed by examining the derivative TGA plots that measured the rate of decomposition directly (see Supporting Information).

Synthesis, Characterization, and Morphology of EVA/Silicate Nanocomposites. As discussed in the preceding section, the high silicate-containing masterbatches prepared from PVAc copolymers containing 1.00 and 2.14 mol % cationic monomer (PVAc-B and PVAc-C series) exhibited the best exfoliation and should make the best candidates for preparing the desired nanocomposites. However, the PVAc-C20 masterbatch nanocomposite, which had the highest AETMC content, was not very miscible with EVA, possibly because of the increased polarity. We also found that the copolymer PVAc-C did not dissolve completely in THF, leading to formation of a somewhat cloudy solution. Therefore, the masterbatch prepared from the copolymer that contained 1.00 mol % cationic monomer, PVAc-B20, which was shown to be mostly exfoliated, was used to prepare the desired nanocomposites. The EVA/silicate nanocomposites (EVA-NC1, -NC2, and -NC5) were, therefore, prepared by adding a THF dispersion of PVAc-B20 masterbatch to a THF solution of EVA and heating the mixture with stirring at 50 °C for 4 h. Evaporation of the solvent to dryness and drying of the residue gave the final nanocomposites in quantitative yields. The higher yields obtained here compared to those obtained for the masterbatches might be due to the minimum handling of the product that required no excessive washings by water or precipitation from large amounts of solvent. For control, PVAc-20 was treated in the same manner to prepare EVA-1, -2, and -5. The compositions of the nanocomposites are summarized in Table 3. Figure 9 shows the XRD plots of the EVA/silicate nanocomposites together with the XRD of pristine MMT.

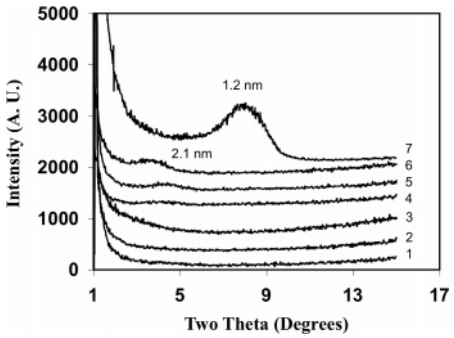

Figure 9. XRD patterns of MMT and EVA/silicate nanocomposites. 1, EVA-NC1; 2, EVA-NC2; 3, EVA-NC5; 4, EVA-1; 5, EVA-2; 6, EVA-5; and 7, MMT.

Comparison of Figures 9 and 3 revealed very clearly that the XRD peak at 4.2° in the intercalated masterbatch (PVAc-20) still remained at the same position for EVA-5 (Figure 9, curve 6). However, the MMT *d*001 peak, which reappeared at 8.3° for PVAc-20, disappeared completely, possibly due to dilution effect that would make it too small to be visible in the XRD of EVA-5. The *d* spacing of 2.1 nm for the peak in the XRD of EVA-5 is larger than the 1.2 nm *d* spacing observed for pristine MMT (Figure 9, curve 7). This suggests that the intercalated structure of the masterbatch (PVAc-20) is retained in the control sample. In the XRD of control samples EVA-1 and EVA-2 that contained only l.2 and 2.3 wt % silicate, respectively, the peaks at 4.2° appeared only as small bumps (Figure 9, curves 4 and 5). However, the fact that these peaks are visible suggests that XRD is sensitive enough to detect as low as 1 wt % non-exfoliated MMT. In contrast, for EVA-NC1 (Figure 9, curve 1), -NC2

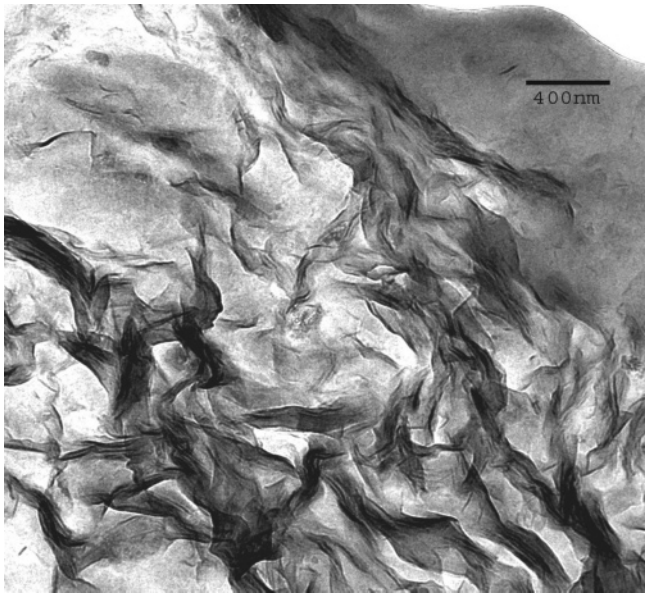

Figure 10. Low magnification TEM of EVA-5.

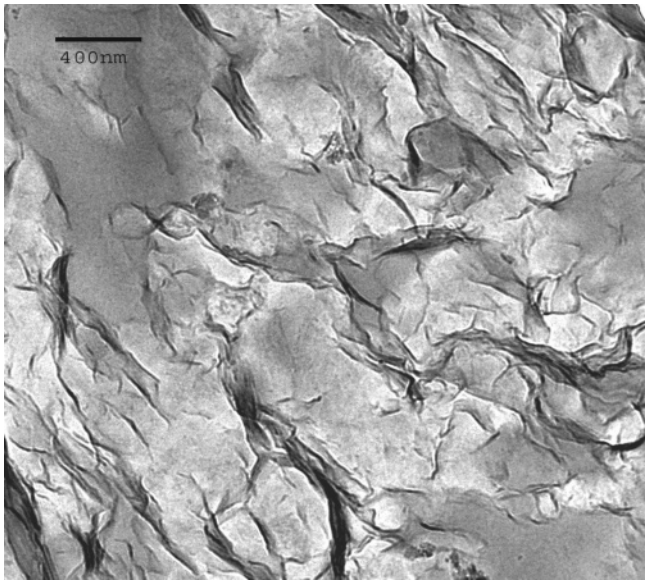

Figure 11. Low magnification TEM of EVA-NC5.

(Figure 9, curve 2), and -NC5 (Figure 9, curve 3), the broad shoulder in the XRD of the PVAc-B20 masterbatch (Figure 3) with *d* spacing of 2.4 nm disappeared, which suggests that these nanocomposites have exfoliated nanostructure. The results also suggest that the broad shoulder represents no more than 1 wt % of non-exfoliated silicate.

The above XRD observations were corroborated by electron microscopy. The TEM image of EVA-5 (Figure 10) revealed mostly stacks of silicate layers in addition to single and double layers, which is in good agreement with the presence of a peak in the XRD (Figure 9). This is clearly an intercalated morphology. In contrast, the TEM of EVA-NC5 (Figure 11) showed mostly well-distributed single or double silicate layers. This is consistent with the absence of XRD peaks and confirms that EVA-NC5, indeed, has exfoliated nanostructure. The results lend credence to the concept of masterbatches as a route to exfoliated nanocomposites, provided, however, that there exists a viable synthetic methodology for the exfoliated masterbatch that contains very high inorganic loading and remains exfoliated throughout its use.

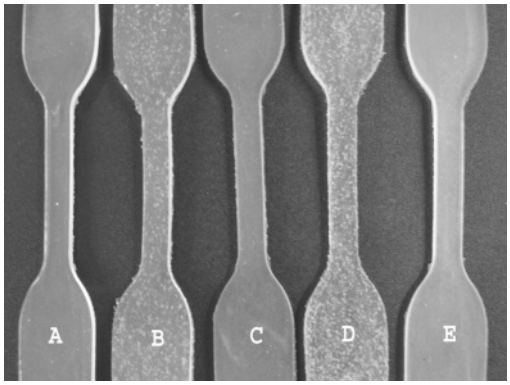

Figure 12. Injection-molded specimens from EVA and its nanocomposites. (A) EVA, (B) EVA-1, (C) EVA-NC1, (D) EVA-2, and (E) EVA-NC2.

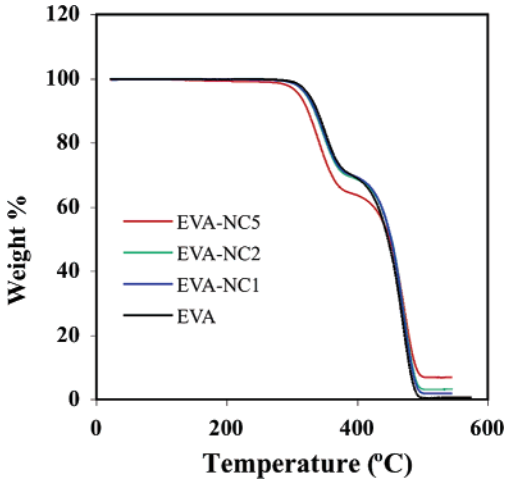

Figure 13. TGA of EVA (black), EVA-NC1 (blue), EVA-NC2 (green), and EVA-NC5 (red) in nitrogen.

Further evidence for the homogeneous morphology of the nanocomposites was obtained by preparing injection-molded specimens from both the exfoliated and the intercalated nanocomposites and comparing the homogeneity and optical clarity with those of injection-molded samples of EVA. It can be seen from Figure 12 that EVA-NC1 (C) and EVA-NC2 (E) are similar to EVA (A) in homogeneity and optical clarity. In contrast, the injection-molded bars prepared from the intercalated nanocomposites EVA-1 (B) and EVA-2 (D) showed silicate particulates, which is completely consistent with the presence of stacks of intercalated silicate layers observed in the TEM of the appropriate masterbatch.

Thermal Stability of EVA/Silicate Nanocomposites in Nitrogen and Air. Figure 13 shows the TGA of the nanocomposites prepared from the masterbatches performed under nitrogen atmosphere. The thermal behavior was similar to what was observed for the masterbatches in that all samples showed the two degradation steps. The degradation temperatures obtained in nitrogen are listed in Table 3. The first onset decomposition temperatures for the exfoliated EVA-NC5 (311 °C) and that for the intercalated EVA-5 (311 °C) were lower than that obtained for pure EVA (322 °C). However, these temperatures are close to those obtained for their respective control samples EVA-NC0 (309 °C) and EVA-0 (309 °C), which suggests that the lower

decomposition temperature is due to the presence of the additional PVAc and that the catalytic effect of the silicate on the deacetylation of both the PVAc modifier and EVA is no longer significant. It appears that the PVAc chains attached to the silicate layers in the masterbatch somewhat shield the EVA from the direct influence of the silicate. This is precisely the essence of the masterbatch concept. For the nanocomposites containing 1−2 wt % silicate (EVA-NC1 and EVA-NC2), the catalytic effect of the silicate was essentially nonexistent as the thermograms overlapped with the curve for pure EVA.

As observed for the masterbatches, T_{d2} was not affected by the silicate as the onset decomposition temperatures remained essentially constant around 444 ± 1 °C. These results are in good agreement with those reported in the literature. For example, Beyer[5] obtained about 15 °C decrease in the first onset decomposition temperature for EVA/silicate nanocomposites containing 5 wt % MMT modified with octadecylammonium salt but found that the second decomposition temperature was unaffected by the presence of the silicate. Zanetti et al.[7] found that while the onset decomposition temperature for the deacetylation reaction of similar nanocomposites containing 10 wt % MMT also modified with octadecylammonium salt was 30 °C lower than that of pure EVA the second decomposition temperatures were unchanged. Riva et al.[13] studied the same nanocomposite containing 10 wt % MMT modified with methyl tallow bis-(2-hydroxyethtyl)ammonium salt and obtained essentially the same results.

Unlike the results in the literature cited above,[5,7,15] the acceleration of deacetylation was not observed for the EVA nanocomposites prepared from pre-exfoliated masterbatches described herein (see Supporting Information). The main explanation provided by the various authors for the acceleration was Brønsted acid catalysis.[7] The acid catalyst is usually formed as a result of the ammonium cationic modifiers (the surfactants) undergoing the well-known Hoffmann elimination reaction. The elimination, which occurs at approximately 200 °C for the surfactants typically used to modify MMT, produces not only amines and other volatiles, such as olefins, but also protons that replace the ammonium groups on the clay surface, thus rendering the clay surface acidic. The EVA nanocomposites contained PVAc that contained low amounts of trimethylammonium cation and did not show any evidence of thermal decomposition below 300 °C. In addition, the sterically congested environment provided by the polymeric modifier could hinder the elimination reaction and, thus, minimize the generation of protons on the silicate surface. These, together with the aforementioned shielding influence of the silicate-anchored PVAc, would reduce both the Brønsted and Lewis acid catalytic effects of the silicate. Hence, the EVA nanocomposites described herein might be expected to start to deacetylate at higher temperatures than those prepared from low molecular weight surfactant-modified silicates. Clearly, the reduction in thermal stability promoted by the degradation byproducts of low molecular weight surfactants can be minimized by using polymeric surfactant modifiers as demonstrated by the results reported herein.

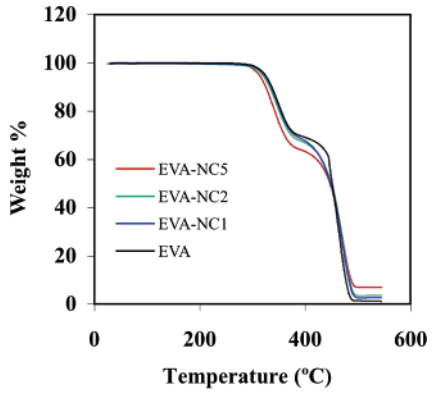

Figure 14. TGA of EVA (black), EVA-NC1 (blue), EVA-NC2 (green), and EVA-NC5 (red) in air.

TGA performed in air is shown in Figure 14. Comparison of the thermograms in Figure 14 with those in Figure 13 revealed that the effect of the silicate on the first thermal oxidation step of the exfoliated nanocomposites (EVA-NC1, -NC2, and -NC5) and pure EVA was the same under both air and nitrogen. In contrast, the second onset decomposition temperatures were 5−10 °C higher than that observed for neat EVA and increased with increasing silicate content. The results suggest that the silicate layers protect the incorporated polymers from thermo-oxidative processes, thereby enhancing thermal stability in air. These results are in general agreement with results reported in the literature.[5,7,13] The TGA of the corresponding intercalated nanocomposites EVA-1, -2, and -5 in air and nitrogen (see Supporting Information) gave results similar to those obtained for EVA-NC1, -NC2, and -NC5. In absence of silicate, the second thermal decomposition event of pure EVA (i.e., decomposition of the ethylene-*co*-acetylene backbone) occurred at slightly lower temperature in air than in nitrogen. Others have reported a much higher decrease (40 °C) in the temperature for the second degradation step for pure EVA in air compared to degradation under nitrogen atmosphere. For example, Zanetti et al.[7] reported the second peak for maximum rate of degradation for EVA at 429 °C in air and 468 °C in nitrogen. Using temperatures for maximum decomposition rates obtained from TGA derivative plots (see Supporting Information) we found the decomposition temperature difference of approximately 23 °C. A closer examination of the TGA thermograms in ref 7 revealed that the change in the second onset decomposition temperature (not peak temperature) was only about 5−10 °C. Using onset of decomposition temperatures for comparing relative stability (thermodynamics) is, in our view, more appropriate than using peak temperatures of maximum decomposition rate which is a kinetic quantity. It is also instructive to point out that the EVA used in the other studies referred to above was EVA19 (19% VAc) in contrast to EVA39 (39% VAc) used in our studies. The higher the VAc content, the higher the level of unsaturation in the backbone after deacetylation and, consequently, the lower the thermo-oxidative temperature.

Dynamic Mechanical Properties of EVA/MMT Nanocomposites. Table 4 summarizes the storage modulus (E') and tan δ of EVA and EVA/silicate nanocomposites at T_g and 15 °C. The temperature dependence of tan δ and storage modulus are plotted in Figures 15 and 16, respectively.

Table 4. Dynamic Mechanical Properties of EVA and Its Nanocomposites

sample	MMT[a] (wt %)	T_g (°C)	storage modulus (E', MPa) at T_g	storage modulus (E', MPa) at 15 °C	tan δ[b] at T_g	tan δ[b] at 15 °C
EVA	0	−17.4	129	7.0	0.54	0.05
EVA-0[c]	0	−16.2	186	15.7	0.48	0.12
EVA-1	0.9	−17.6	122	8.3	0.52	0.08
EVA-2	1.9	−16.7	131	8.7	0.56	0.07
EVA-5	5.9	−18.9	272	17.2	0.51	0.13
EVA-NC0[d]	0	−16.9	206	18.1	0.49	0.13
EVA-NC1	0.84	−17.6	142	9.7	0.56	0.09
EVA-NC2	2.1	−18.3	157	11.2	0.48	0.10
EVA-NC5	5.6	−17.9	290	30.7	0.41	0.15

[a] Measured by TGA. [b] Measured as peak height. [c] Contains EVA (80 wt %) and PVAc (20 wt %). [d] Contains EVA (80 wt %) and PVAc-B (20 wt %).

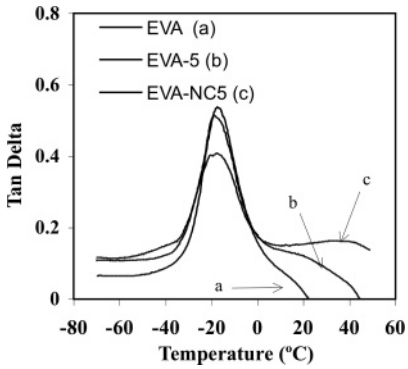

Figure 15. tan δ of EVA and EVA/silicate nanocomposites EVA-5 and EVA-NC5.

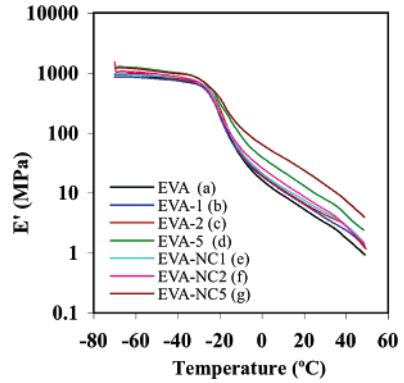

Figure 16. Storage modulus versus temperature plots for EVA and its nanocomposites. EVA, black (a); EVA-1, blue (b); EVA-2, red (c); EVA-5, green (d); EVA-NC1, light blue (e); EVA-NC2, purple (f); and EVA-NC5, brown (f).

Examination of the tan δ plots and the data in Table 4 revealed that the dynamic T_g values of the nanocomposites did not change significantly compared with the T_g of neat EVA. Upon addition of PVAc to form EVA-0, T_g of EVA increased slightly from −17.4 to −16.2 °C. Similarly, addition of the copolymer to form EVA-NC0 led to a very small increase in T_g. However, upon addition of the silicate the T_g decreased, with EVA-5 exhibiting the lowest value (−18.9 °C). A similar trend was observed for the exfoliated nanocomposites. Thus, as the masterbatch nanocomposite was added to EVA the T_g changed as follows: −17.6 °C for EVA-NC1, −18.3 °C for EVA-NC2, and −17.9 °C for EVA-NC5. These changes are small, suggesting that the influence of the silicate on the thermal transitions is not significant. This is possibly due to the fact that in these nanocomposites the EVA chains interact mainly with the PVAc attached to the silicate. This is the main premise of the masterbatch concept, that is, to minimize the incompatibility between the main organic polymer matrix and the hydrophilic silicate by inserting a polymeric modifier that is compatible with both the polymer matrix and the silicate.

The tan δ peak (T_g) reflects polymer segmental motion in the amorphous domain. However, the T_g values of the EVA/silicate nanocomposites will be influenced not just by the amorphous domain of EVA but also by (a) the additional PVAc from the masterbatch and (b) the silicate. On one hand, since PVAc has a higher T_g than EVA, one might expect the addition of PVAc to EVA to lead to an increase in T_g. On the other hand, the crystalline domain of the polyethylene component of EVA would be reduced by the addition of amorphous PVAc and clay, as supported by literature reports.[28,29] This would be expected to result in lower T_g. In addition, the impact of clay on T_g of polymer/clay nanocomposites can be in either direction.[30,31] In our case, the addition of silicate caused lowering of the T_g. Hence, it appears there is some cancellation of the two opposing effects, leading to essentially no change in the T_g.

As can be seen in Figure 15, the heights of tan δ peaks for neat EVA and EVA-5 are very close to each other, although the latter is broader. In contrast, the EVA-NC5 nanocomposite with almost the same silicate content showed a much smaller but broader transition peak than all samples. Closer examination of the tan δ peaks revealed a clear trend of decreasing peak height with increasing silicate content. Thus, the height of the tan δ peak decreased from 0.49 for EVA-NC0 (control) to 0.41 for EVA-NC5 (Table 4). In comparison, the heights of tan δ peaks for EVA-1, -2, and -5 were close to the value for neat EVA, which might be associated with the inhomogeneity of the intercalated structure of these nanocomposites. One possible explanation for these observations is that in EVA-NC5, the EVA polymer chains had slightly more restricted mobility because of their interaction with the PVAc chains anchored to the silicate. However, in EVA-5, the PVAc chains were not attached to the silicate, and the mobility of the EVA chains was not confined in the same way as in EVA-NC5. Evidently, this effect is enough to cause broadening and, hence, reduction of intensity of the glass transitions but not enough to significantly affect the transition temperature. Pramanik et al.[18] also reported decreased heights of tan δ peaks upon increasing MMT levels that were similarly accompanied by only small changes (3−5 °C) in T_g.[18,32]

To determine effect of the silicate on storage modulus, DMA was carried out. Figure 16 shows the storage modulus−

(28) Gopakumar, T. G.; Lee, J. A.; Kontopoulou, M.; Parent, J. S. *Polymer* **2002**, *43*, 5483−5491.
(29) Wang, K. H.; Choi, M. H.; Koo, C. M.; Xu, M.; Chung, I. J.; Jang, M. C.; Choi, S. W.; Song, H. H. *J. Polym. Sci., Part B: Polym. Phys.* **2002**, *40*, 1454−1463.
(30) McNally, T.; Raymond Murphy, W.; Lew, C. Y.; Turner, R. J.; Brennan, G. P. *Polymer* **2003**, *44*, 2761−2772.
(31) Abot, J. L.; Yasmin, A.; Daniel, I. M. *MRS Symp. Proc.* **2002**, *740*, 167−172.
(32) These authors also explained their data by the restricted mobility hypothesis but incorrectly referred to the glass transition peak as β relaxation instead of α relaxation.

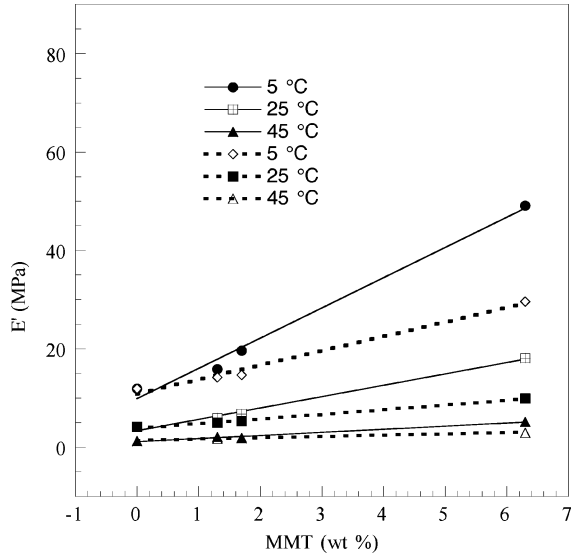

Figure 17. Storage moduli versus MMT content for EVA-NC0, -NC1, -NC2, and -NC5 (solid lines) and EVA-0, EVA-1, EVA-2, and EVA-3 (dotted lines) at different temperatures.

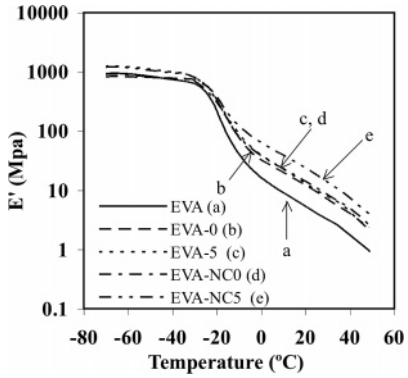

Figure 18. Storage modulus versus temperature plots for EVA/silicate nanocomposites and EVA/PVAc blends. EVA, solid line (a); EVA-0, dashed line (b); EVA-5, dotted line (c); EVA-NC0, dash-dotted line (d); and EVA-NC5, dash-double-dotted line (e).

temperature plots for the various nanocomposites. Figure 17 shows the plots of storage modulus versus silicate content at selected temperatures for the EVA-NC series. In general, the nanocomposites showed enhancement in modulus compared to EVA. This effect depended on the MMT loading. Thus, for each series the storage modulus increased as the silicate content increased. Furthermore, at temperatures above T_g, the storage moduli of the exfoliated nanocomposites (EVA-NC1, -NC2, and -NC5) were higher than those of the corresponding intercalated nanocomposites (EVA-1, -2, and -5) containing comparable amounts of silicate (Figure 16). For example, at 15 °C the storage modulus of EVA-NC5 increased 4.4 times that of EVA compared to the 2.4-fold improvement for EVA-5 (Table 4). This reinforces the premise that the extent of exfoliation of the silicate layers plays a significant role in property improvements.

An important question arises regarding the relative contributions of both the silicate and the PVAc copolymer from the masterbatch to the observed differences in properties. To address this question, we prepared EVA/PVAc blends without adding MMT and measured their dynamic mechanical properties (Figure 18). The composition and properties are summarized in Table 5. EVA-0 contained about 20 wt % PVAc while EVA-NC0 contained about 20 wt % of the copolymer very close to the actual polymer contents in the corresponding EVA-5 and EVA-NC5 nanocomposites, respectively. The storage moduli of EVA-5, EVA-NC5, and the corresponding blends EVA-0 and EVA-NC0 are plotted in Figure 18.

Table 5. EVA/MMT Composites and Corresponding EVA/PVAc Blends

nanocomposite	masterbatch	PVAc wt %	MMT wt % (TGA)	T_g (°C)	E' (MPa) at 15 °C	tan δ at 15 °C
EVA	N/A	0	0	−17.4	7	0.05
EVA-0	PVAc	20	0	−16.2	15.7	0.12
EVA-5	PVAc-20	20	5.9	−18.9	17.2	0.13
EVA-NC0	PVAc-B	20	0	−16.9	18.1	0.13
EVA-NC5	PVAc-B20	20	5.6	−17.9	30.7	0.15

Clearly, upon addition of just PVAc or cationic PVAc copolymer to EVA the storage modulus increased by more than a factor of 2 (2.4 for EVA-0 and 2.5 for EVA-NC0). This suggests that the component polymers contribute significantly to the property improvement, with the copolymer being slightly more effective than PVAc. Further improvement was observed upon addition of MMT. Thus, the storage modulus of EVA-5 increased by factors of 2.6 and 1.1 over the storage modulus of EVA and that of the blend EVA-0, respectively. The exfoliated nanocomposite, EVA-NC5, showed the most improvement in storage modulus, increasing by factors of 4.4 and 1.7 over the storage modulus of EVA and that of the corresponding blend EVA-NC0, respectively, and by a factor of 1.8 over that of the intercalated EVA-5 nanocomposite. Therefore, the improvement in storage modulus was due to the synergistic effect of the silicate and the polymer incorporated into the masterbatch, and the improvement was highest when the silicate was well exfoliated in the polymer matrix. Zhang et al.[11] studied a series of EVA/MMT nanocomposites and macrocomposites using EVA containing different amounts of VAc (28, 40, 50, 80%) and observed a 50−62% increase in the storage modulus. It is worth mentioning that although there are some reports on morphology studies of EVA/PVAc blends,[20−22] we have not seen any dynamic mechanical or mechanical property studies on this system, making this the first report of such studies of EVA/PVAc blends.

DMA is a very useful tool to measure viscoelastic properties of polymer materials and can often be used as a good predictor for mechanical behaviors. The exfoliated EVA nanocomposites in this work demonstrated very good mechanical properties and flame retardant properties, which will be reported in a separate manuscript.

Summary and Conclusions

VAc was copolymerized with AETMC to give cationic PVAc containing 0.37, 1.0, and 2.14 mol % cationic units. The cationic polymers were used to synthesize PVAc/MMT masterbatch nanocomposites, which showed complete exfoliation at very high silicate contents. These PVAc/MMT nanocomposites were used as masterbatches to make EVA nanocomposites via solution blending with EVA. XRD and (S)TEM confirmed the existence of exfoliated structures. The storage modulus of the nanocomposites was improved by

synergistic effect of the PVAc (co)polymer and the silicate. For example, the EVA nanocomposite containing 5.6% MMT showed a storage modulus of 4.4 times that of pure EVA and 1.7 times that of the EVA/PVAc blend. As a comparison, when PVAc homopolymer was used to make intercalated EVA nanocomposites, the improvement in storage modulus was much smaller. Hence, the approach of using cationic PVAc copolymer to modify MMT was very successful in producing exfoliated EVA/silicate nanocomposites with superior dynamic mechanical properties compared to unfilled EVA polymer.

Acknowledgment. This research was, in part, funded by NSF under Grant DMF-0079992 and Hercules, Incorporated, through the Polymer Outreach Program of Cornell Center for Materials Research. Particular acknowledgment is made of the use of the XRD, STEM, SEC, TGA, and DSC Facilities of the CCMR. The STEM laboratory is supported by the Cornell Center for Materials Research (NSF DMR-9632275). The HB501 UHV-STEM was acquired through the National Science Foundation (Grant DMR-8314255). The authors thank Mr. Mick Thomas for the help with STEM measurements and Dr. Maura Weathers for help with XRD tests. The authors are also grateful to Exxon Mobil for providing the EVA samples.

Supporting Information Available: Experimental procedures for copolymerization of VAc with AETMC, synthesis of PVAc/MMT masterbatch and EVA/silicate nanocomposites, table of rates of decomposition from slopes of decomposition curves, and TGA plots for EVA39, masterbatch nanocomposites, and EVA/silicate nanocomposites both under nitrogen and air together with the corresponding derivative plots (PDF). This material is available free of charge via the Internet at http://pubs.acs.org.

CM060593Y